Published in final edited form as:
Mol Psychiatry. 2022 June 01; 27(6): 2766–2776. doi:10.1038/s41380-022-01527-5.

Targeted Therapy of Cognitive Deficits in Fragile X Syndrome

A. Puścian[1,2,3,*], **M. Winiarski**[1,3], **J. Borowska**[1], **S. Łęski**[1], **T. Górkiewicz**[1,3], **M. Chaturvedi**[1,4], **K. Nowicka**[1,3], **M. Wołyniak**[1], **J.J. Chmielewska**[5,6], **T. Nikolaev**[1,3], **K. Meyza**[1,3], **M. Dziembowska**[5], **L. Kaczmarek**[1,3], **E. Knapska**[1,3,*]

[1]Nencki Institute of Experimental Biology of Polish Academy of Sciences, Warsaw, Poland

[2]Yale School of Medicine, Department of Neuroscience, New Haven, CT, United States

[3]Center of Excellence for Neural Plasticity and Brain Disorders: BRAINCITY, a Nencki-EMBL Partnership

[4]Kennedy Institute of Rheumatology, University of Oxford, Roosevelt Drive, Headington, Oxford, UK

[5]Laboratory of Molecular Basis of Synaptic Plasticity, Centre of New Technologies, University of Warsaw, Warsaw, Poland

[6]Postgraduate School of Molecular Medicine, Medical University of Warsaw, Warsaw, Poland

Abstract

Breaking an impasse in finding mechanism-based therapies of neuropsychiatric disorders requires a strategic shift towards alleviating individual symptoms. Here we present a symptom and circuit-specific approach to rescue deficits of reward learning in *Fmr1* knockout mice, a model of Fragile X syndrome (FXS), the most common monogenetic cause of inherited mental disability and autism. We use high-throughput, ecologically-relevant automated tests of cognition and social behavior to assess effectiveness of the circuit-targeted injections of designer nanoparticles, loaded with TIMP metalloproteinase inhibitor 1 protein (TIMP-1). Further, to investigate the impact of our therapeutic strategy on neuronal plasticity we perform long-term potentiation recordings and high-resolution electron microscopy. We show that central amygdala-targeted delivery of TIMP-1 designer nanoparticles reverses impaired cognition in *Fmr1* knockouts, while having no impact on deficits of social behavior, hence corroborating symptom-specificity of the proposed approach. Moreover, we elucidate the neural correlates of the highly specific behavioral rescue by showing that the applied therapeutic intervention restores functional synaptic plasticity and

*Correspondence to: e.knapska@nencki.edu.pl phone: +48225892370, a.puscian@nencki.edu.pl phone: +48225892290, Nencki Institute of Experimental Biology of Polish Academy of Sciences, Pasteur 3 Street, 02-093, Warsaw, Poland.

Authors contributions: Concept and design A.P., E.K.; data acquisition A.P., M.W., J.B., T.G., M.C., M.W., J.J.C, T.N., K.M., M.D.; analysis and interpretation of data A.P., M.W., S.Ł., T.G., T.N., K.M., L.K., E.K.; drafting and revising the article A.P., K.M., L.K., E.K. We are thankful to Thomas G. Custer and Katie Ferguson for the critical reading of the manuscript and to Svitlana Antoniuk for the invaluable technical support.

Conflict of interest
The authors declare no competing financial interests in relation to the work described.

Europe PMC Funders Author Manuscripts

ultrastructure of neurons in the central amygdala. Thus, we present a targeted, symptom-specific and mechanism-based strategy to remedy cognitive deficits in Fragile X syndrome.

Introduction

Contemporary psychiatry struggles with proposing effective, mechanism/neuronal circuit-based therapies of neurodevelopmental disorders [1]. The major problem to be solved is the heterogeneity of symptoms displayed by people with the same diagnosis. Even in diseases of a well-known genetic origin, such as Fragile X Syndrome (FXS) resulting from the loss of function mutations of *FMR1* gene, symptoms vary from patient to patient [2–5]. Thus, it is crucial to be able to treat particular deficits, rather than elusive FXS phenotype as a whole. To accelerate the search for effective treatments, a shift of focus towards appreciation of the individual phenotype is needed. Such approach is recommended by the National Institute of Mental Health in the current Research Domain Criteria (RDoC) framework [6]. Here we propose a symptom- and neuronal circuit-specific, a mechanism-based strategy to rescue cognitive deficits in a well-validated mouse model of FXS, the *Fmr1* knock-out mice (KO).

FXS is the most common monogenetic cause of inherited mental disability and autism, with a wide range of symptoms in cognitive and social domains [2]. FXS patients and *Fmr1* KO animals lack a fully functional copy of *Fmr1* gene. This leads to the deficiency of its product, the FMRP protein, a key translation suppressor of numerous synaptic molecules, resulting in their upregulation. One of the upregulated proteins is matrix metalloproteinase-9 (MMP-9) [7], a locally translated enzyme, involved in the activity-dependent reorganization of the dendritic spine architecture necessary for memory formation and learning [8–13]. The critical role of MMP-9 hyperactivity in the manifestation of FXS symptoms [14, 15] sparked several attempts to regulate enzyme's levels in both, *Fmr1* KO animals and FXS patients [16–21]. Among the most promising were the crossing of the *Fmr1* KO and the *Mmp9* KO mice [22] and treatment trials with minocycline, a wide spectrum antibiotic that unselectively inhibits MMP-9 expression and activity [15, 23, 24]. Importantly, some clinical trials have reported that minocycline has beneficial effects on reducing symptoms in FXS subjects [25–28]. Although described attempts show that inhibition of overly active MMP-9 is a promising strategy for alleviating FXS symptoms, long term minocycline treatment has pernicious side effects [29–31] and thus cannot be considered a conceivable permanent treatment.

The convergence of progress in targeted inhibition of matrix metalloproteinases [32–34] and automated behavioral testing, which enables a reliable, high-throughput assessment of FXS phenotypes, has raised a possibility of evaluating such new therapeutic strategies. Here we combine a designer tissue inhibitor of metalloproteinases (TIMP-1) delivery system with long-term potentiation (LTP) experiments, and high-resolution electron microscopy, to test the effects of the treatment at the level of functional neuronal circuit. TIMP-1 is an enzyme inhibiting the activity of matrix metalloproteinases, i.a. MMP-9 and disintegrin-metalloproteinases [35–38]. The former determines its key role in regulation of the extracellular matrix composition and function [33, 34]. Here we use the TIMP-1-loaded designer nanoparticles to evoke the non-selective MMP-9 inhibition, resembling that

Europe PMC Funders Author Manuscripts

Europe PMC Funders Author Manuscripts

resulting from the minocycline treatment, however, limited to a particular neuronal circuit and thus of a targeted character. Further, we elucidate how this symptom- and circuit-specific approach, aimed at the relevant molecular mechanism, constitutes an advance in rescuing FXS phenotypes.

Our approach combines the innovative phenotype assessment with a pharmacological intervention of a translational potential, the use of designer nanoparticles (NPs). Indeed, targeted nanoparticles are already considered a promising tool in diagnosis and treatment of cancer [39–42] and some autoimmune diseases [43–46]. Here we use NPs to selectively deliver TIMP-1 into the central amygdala (CeA), where the protein is then gradually released from the polymer over several days, thus mimicking prolonged drug delivery. As shown by Chaturvedi at al., over 50% of the inhibitor load is released after 5 days from its delivery. Then TIMP-1 cumulative release plateaus on day 8th at around 70% and is sustained at this level for the next two weeks[34]. Due to employment of fully automated behavioral testing we are able to design protocols measuring cognition and social interaction narrowed to that period. Finally, the NP's are fluorescently tagged with FITC allowing for the precise verification of the drug-release site.

We show that local, CeA-restricted, release of TIMP-1 not only ameliorates severe deficits of reward learning in *Fmr1* KOs, but also normalizes the circuit physiology, ultrastructure of synapses and dendritic spines. Our intervention restores functional neuronal plasticity and synaptic morphology within the CeA. As previously shown, abnormal activity of MMP-9 in the CeA selectively disrupts cognitive abilities based on reward learning [47]. Moreover, it was discovered that the basolateral-CeA circuits play a critical role in promoting appetitive behavior [48]. Notably, applied therapeutic strategy has no impact on impaired social behavior, corroborating symptom-specificity of the proposed approach.

Materials and Methods

For a more detailed description of the Materials and Methods please see Supplementary Information.

Animals

Animals were treated in accordance with the ethical standards of the European Union (directive no. 2010/63/UE) and Polish regulations. All experimental procedures were pre-approved by the Local Ethics Committee. *Fmr1* KO mice of the FVB strain (FVB.129P-*Fmr1*^{tm1Rbd}/J) and respective littermate controls were bred at the Animal House of the Nencki Institute of Experimental Biology, Poland. Since male *Fmr1* KOs showed high levels of aggression females were used in all experiments. Mice were 2-months-old at the beginning of the experimental procedures. The number of animals used in particular experiments is reported in the figures' descriptions. For details on housing conditions and electronic tagging protocol please refer to the Supplementary Information.

Poly(DL-lactide-co-glycolide) nanoparticles containing TIMP-1 or BSA

To deliver TIMP-1, a non-selective endogenous MMP-9 inhibitor, to the CeA, we used poly(DL-lactide-co-glycolide) (PLGA) nanoparticles (NPs, 19,20). NPs gradually release

TIMP-1 in the tissue, reducing MMP-9 activity for at least several days [34]. As described by Chaturvedi et. al. multiple emulsion and solvent evaporations were applied for synthesis of TIMP-1 or BSA-loaded (control conditions) PLGA NPs (MW 45,000–75,000; copolymer ratio, 50:50; Sigma-Aldrich). 5 ml dichloromethane was used to dissolve 100 mg of PLGA (50:50) and 4 mg of dimethyl tartaric acid (Sigma-Aldrich). To facilitate the release of TIMP-1 or BSA encapsulated in the NPs dimethyl tartaric acid was used. One mg of TIMP-1 or 1 mg of BSA (Sigma-Aldrich) was dissolved in 500 μl of MiliQ water and BSA was used to stabilize the encapsulated enzyme and prevent it from interfacial inactivation. FITC was encapsulated in NPs along with the respective proteins to localize the injection site after the NPs had been delivered to the brain. Next, to make a primary emulsion, a probe sonicator was used to emulsify the protein solution in to dichloromethane containing PLGA. This primary emulsion was further emulsified in 20 ml of 1% polyvinyl alcohol (on average MW 30,000–70,000; Sigma-Aldrich) in MiliQ water. To evaporate dichloromethane, the solution was stirred in RT o/n. Afterwards NPs were collected by centrifugation at 10,000×g and washed three times with MiliQ water. To obtain a ready-to-use solution, NPs were dissolved in PBS and stored at 4° C.

Stereotaxic surgeries

We delivered NPs into the CeA (coordinates AP: −1.1 mm; LM: ±2.6 mm; DV: −5.3 mm) bilaterally with a Nanofil 26G beveled needle. After surgery, mice were placed in the home cages and singly-housed for the next 48-72 h, before being returned to their experimental cohort. For more details of this protocol please see Supplementary Information.

In-situ zymography

Five days after surgeries brain slices from *Fmr1* KO and WT mice were first pre-incubated in water at 37°C for 100 min, and then overlaid with a fluorogenic substrate DQ™-gelatin (Thermo Fisher, United States) diluted 1:100 in the buffer supplied by the manufacturer. DQ gelatin was used to detect MMP-9 activity in vitro with high sensitivity. Upon proteolytic digestion, bright green fluorescence revealed MMP-9 gelatinase activity. Finally, the slides were washed with PBS, dried overnight and mounted (Fluoromount-G, SouthernBiotech, United States), and subsequently imaged under the Nikon Eclipse Ni microscope. Fluorescence intensity was measured in ImageJ software. For more details of this protocol please see Supplementary Information.

Detection of MMP-9 activity with a A580 MMP Substrate 1

Five days after surgery mice were anesthetized with isoflurane and decapitated. The brains were removed and sliced using a Leica VT1200s vibratome in 4°C artificial cerebrospinal fluid (ACSF) of the following composition (in mM): 119 NaCl, 2.5 KCl, 2 $MgSO_4$, 2 $CaCl_2$, 1.25 NaH_2PO_4, 26 $NaHCO_3$, 10 D-glucose equilibrated with 95% O_2/5% CO_2 gas composition. 150-μm-thick coronal slices containing CeA were collected and incubated for 30 min in ACSF with A580 MMP Substrate 1 (1 μg/ml, Anaspec) at RT. A580 MMP Substrate 1 is a small synthetic peptide (QXL 570 - KPLA - Nva - Dap(5 - TAMRA) - AR - NH2) in which fluorescence emission is blocked by the intramolecular quenching (from TAMRA to QXL). When the peptide is cleaved by MMP2/9, intramolecular FRET is disrupted, causing emission of fluorescence following excitation at 545 nm. After incubation

with biosensor, the slices were washed in ACSF and fixed in 4% PFA for 3 hours and washed 3x in PBS, mounted on slides and covered with Fluoromount-G with DAPI (Invitrogen). Regions of interest, that is square-shaped areas of approx. 120x120 μm inside of the central amygdala were imaged as z-stacks with 63x oil objective on ZEISS Spinning DISC confocal microscope (488nm channel to localize sites of the NPs injections as tagged with FITC, and 555nm channel for the signal of A580 MMP Substrate 1) and subjected to the analysis. Image analysis was performed with ImageJ. The threshold settings were normalized to the background of each image individually. The signal area was measured based on maximum intensity projection of z-stacks [49].

High throughput, automated and ecologically-relevant behavioral testing

Cognitive assessment - reward learning—*Fmr1* KO and WT animals injected with the NPs releasing TIMP-1 or BSA were subjected to a 15-day IntelliCage protocol during which they were continuously housed in the system in cohorts of 7-12 mice. During that time animals had unconstrained and unlimited access to all the conditioning units placed in the corners of the IntelliCage apparatus. The protocol was divided in two parts separated by a 3-day period of surgery and recovery. First, animals were adapted to the experimental environment during a ‘simple adaptation’ phase (4 days), ‘nosepoke adaptation’ phase (2 days), and ‘preparatory place learning’ phase (3 days). At this time all drinking bottles contained tap water. During ‘simple adaptation’, doors in all conditioning units (corners) were open and access to water was unrestricted. During the following ‘nosepoke adaptation’, all doors were closed by default and opened when an animal put its snout (nosepoke response) into one of the two holes on the operant learning chamber’s walls. The door remained open as long as the animal kept its snout in the hole, regardless of drinking behavior. During ‘preparatory place learning’, access to drinking bottles was restricted to a single conditioning unit. A chamber with access to water was assigned randomly, with no more than 3 mice drinking from the same conditioning unit. Such design has been shown to limit social modulation of learning [50]. Additionally, due to the design of the entrances (a short tube-shaped corridors, approx. 4cm in diameter) only one animal was able to get into the conditional unit at a time. Since only 3 mice from the tested groups were assigned to be able to obtain the reward by nosepoking in each of the units and they could enter them whenever they were free over the course of the entire day-light cycle for 5 subsequent days the competition for the resources was practically nonexistent.

Next, animals were subjected to the stereotaxic surgery during which TIMP-1- or BSA-loaded NPs were bilaterally injected into the CA. After surgery animals were singly-housed for 72 hours to ensure recovery. Afterwards, mice were put back into the same IntelliCage where they were housed onwards. First, mice were subjected to the one-day of ‘preparatory place learning’, to ensure they were able to successfully find the corner with access to water. This phase was followed by reward learning (5 days) starting at the beginning of the TIMP-1 or BSA release (5 days after surgery). The mice then had a choice between nosepoking to the bottle containing tap water or to the bottle containing the reward (10% sucrose solution) placed behind 2 opposite doors in a given conditioning chamber. Correct response was defined as a percentage of nosepokes made to the bottle containing the reward as the first choice after entering the conditioning unit. To avoid potential influence of side-bias on

learning, the reward was always placed in the hole less frequently nosepoked into during the preceding 24h, when both bottles still contained water. Such procedure excludes the possibility that animals performed the instrumental responses habitually, rather than because they were driven by the reward. Additionally, we measured an increase (%) in undirected nosepoking (a proportion of the nosepokes performed within the first 24h after the reward was introduced into the experimental environment to the nosepokes performed during the preceding 24h period), as a parameter reflecting difficulty in learning reward location. Further, for the control purposes we recorded a total number of nosepokes, visits (activity), and liquid consumption.

Two replications of the experiment were performed in TIMP-1-treated *Fmr1* KO and TIMP-1-treated WT littermate mice. 3 replications were performed in control (BSA-treated) *Fmr1* KO and WT littermate mice due to the lower success rate of bilateral CeA targeting. The final number of animals successfully injected and tested were as follows: 8 *Fmr1* KO injected with TIMP-1, 7 *Fmr1* KO injected with BSAs, 8 WT injected with TIMP-1 and 8 WT mice injected with BSA.

Social behavior—2 days after the stereotaxic surgery cohorts of 7-12 *Fmr1* KO and WT animals injected with NPs releasing TIMP-1 or BSA were subjected to the 72-hour Eco-HAB testing protocols divided into an adaptation phase (48 h) and social behavior testing (24 h, approach to social odor and in-cohort sociability) [51]. The testing phase started at the beginning of the peak protein release (5 days after surgery). Access to food and water was unrestricted. During all phases of the experiment mice could freely explore all compartments. During the test of social behavior, olfactory stimuli - bedding from the cage of an unfamiliar mouse of the same strain, sex and age (novel social scent) or fresh bedding (novel non-social scent) were presented in a randomized manner. The opposite testing compartments, in which the olfactory stimuli were placed behind the perforated partitions, were chosen randomly during the first iteration of each experiment and then switched in all the subsequent replications to avoid the influence of place bias on the interpretation of the results.

Social approach was assessed as the ratio of approach to social vs. non-social odor during the first hour after the introduction of the stimulus. The duration of the measurement was chosen based on the activity level of the investigated mouse strain, as previously described [51]. Additionally, in-cohort sociability was assessed during the 24h testing period. In-cohort sociability reflects a tendency to voluntarily spend time with conspecifics. As previously described [51], the value of in-cohort sociability was calculated as a total time each pair of mice spent together minus the time that animals spent jointly, due to their individual preferences for occupying certain spaces within the Eco-HAB. For algorithms allowing for the calculation of both sociability measures in Eco-HAB see [51]. Two replications of the experiment were performed in each experimental group: TIMP-1-treated *Fmr1* KOs, TIMP-1-treated WT littermates, control (BSA-treated) *Fmr1* KOs, and control (BSA-treated) WT littermates. The final number of animals successfully injected and tested were as follows: 6 *Fmr1* KOs injected with TIMP-1, 6 *Fmr1* KOs injected with BSA, 5 WTs injected with TIMP-1 and 8 WTs injected with BSA.

Electrophysiological recordings

Experiments were performed 5 days after surgery in 2.5-3.5-month-old mice injected with FITC-conjugated NP's containing TIMP-1. Field excitatory postsynaptic potentials (fEPSPs) were recorded from the medial part of CeA using a glass pipette filled with 20 mMNaCl (impendence 1.0–3.0 MΩ). To evoke fEPSPs, test pulses at 0.033 Hz, 0.1 ms were delivered to the basal amygdala (BA) with bipolar metal electrodes (FHC, USA). The intensity of test stimulus was adjusted to obtain fEPSP with amplitude that amounted to a half of the maximum response. After at least 15 min of stable baseline recording, a theta burst protocol (TBS) was used to evoke LTP. Three trains of stimuli were applied every 5 min. One train was composed of five sequences of pulses separated by 1 s. Each sequence consisted of five bursts of stimuli at 5 Hz. The bursts consisted of eight pulses at 100 Hz. Basic synaptic transmission, presented as the IO curves, was calculated based on the data obtained as follows. We applied 16 subsequent stimuli of increasing intensity, up to the maximum stimulus value (1mA). Notably, the extracellular recording system used (ISO-FLEX A.M.P.I.) is equipped with a nonlinear stimulus isolator, and thus does not allow for setting up a precise intensity of particular stimuli delivered, hence the x axis in the graphs is labeled with stimuli numbers.

LTP recordings conducted in *Fmr1* KO mice: TIMP-1 group, 7 animals, n=9 slices; CTRL group 7 animals, n=11 slices. LTP recordings conducted in WT mice: TIMP-1 group, 6 animals, n=7 slices; CTRL group, 8 animals, n=9 slices, recording from 1 additional slice was unsuccessful. Basic synaptic transmission (input-output curves) in *Fmr1* KO mice: TIMP-1 group, 7 animals, n=7 slices, recordings from two additional slices were unsuccessful; CTRL group, 7 animals, n=11 slices. Basic synaptic transmission in WT mice: TIMP-1 group, 6 animals, n=7 slices; CTRL group, 8 animals, n=10 slices).

Serial block-face scanning electron microscopy (SBF-SEM)

5 days after stereotaxic surgery *Fmr1* KO and WT mice injected with FITC-conjugated NP's containing TIMP-1 (n=3 per group) and control animals (n=3 per group) were anesthetized, perfused and brains were isolated. CeA-containing tissue cubes (identified in accordance with the Paxinos and Franklin's Mouse Brain Atlas) were further stained and imaged with a use of SBF-SEM Sigma VP 3View electron microscope. Image stacks were reconstructed and analyzed with Reconstruct v.1.1.0.1 (30,31). 4 cubic samples were imaged per animal (vol. 100 μm, 12 samples per group). We calculated the number of synapses and dendritic spines. Synapses were defined as post-synaptic densities (PSDs). Additionally, we calculated shafts, synapses without any dendritic spine structure. Dendritic spines were defined as morphologically mature (mushroom-shaped) or immature (filopodial or stubby). Spines containing 2 and more PSDs or connecting to 2 or more presynaptic bulbs were defined as multi-innervated.

Statistical analysis

Statistical analyses of data were performed with GraphPad Prism8 software. Normality of data distributions was assessed with D'Agostino-Pearson omnibus normality test or Shapiro-Wilk normality test. When appropriate, group comparisons were analyzed using repeated-measures ANOVA or Student's 2-tailed t-test for independent samples. Datasets

that did not meet the criteria for parametric analyses were compared with the 2-tailed Mann-Whitney U-Test. All statistics for the serial block-face scanning electron microscopy data were calculated across mice. To compare performance in reward learning to chance level (50%), the 2-tailed Wilcoxon signed-rank test was used. Chi-squared tests were performed to compare distributions of singly- and multi-innervated dendritic spines. The criterion for statistical significance was a probability level of $p<0.05$. The specific statistical tests used and legends for presented p values, as well as n values are included in the figures captions, both main and supplementary ones.

Results

Central amygdala-targeted TIMP-1 treatment rescues cognitive but not social deficits in *Fmr1* KO mice

Fmr1 KO mice display MMP-9 upregulation in several brain structures [7–9, 11, 15], a characteristic that is thought to be directly related to their behavioral and cognitive impairments [22–24, 54–57]. The effect is also present in their CeA (Fig. S1), the brain structure whose function is indispensable for the proper reward learning [47, 48]. We show that both elevated MMP-9 activity in the CeA (Fig. S1) and the resulting cognitive deficits (Fig. S3) are alleviated by the targeted injection of the designer nanoparticles (NPs), releasing tissue inhibitor of matrix metalloproteinases-1 (TIMP-1), an endogenous, non-selective MMP-9 inhibitor. To verify symptom-specificity of our approach we also investigated the potential effect of the treatment on social deficits. In all experiments under control conditions, animals were injected with NPs containing the Bovine Serum Albumin (BSA), which has no effect on MMP-9 activity or animal behavior [47, 58–61]. NPs were designed to gradually release TIMP-1 or BSA ~~(as a control)~~ from the polymer over several days, thus mimicking prolonged drug delivery, with over 50% of the inhibitor load being delivered 5 days after the infusion [33, 34].

To reliably assess cognitive and social deficits of *Fmr1* KOs and the effect of the proposed therapeutic strategy we employed fully automated and ecologically-relevant assays of mouse behavior; IntelliCage system to measure cognition, and Eco-HAB to evaluate sociability. Both systems measure spontaneous, voluntary behavior and assert high data reproducibility due to automation and fully standardized conditions [51, 62]. They enabled us to design protocols measuring cognition and social behavior narrowed to the TIMP-1 release period. Prior to the experiments group-housed mice were subcutaneously injected with RFID chips allowing for the individual assessment of their behavior over the course of several-day-long testing protocols. After adaptation to the respective experimental environments *Fmr1* KO and WT animals were stereotactically injected with the FITC-tagged NPs containing TIMP-1 or BSA, bilaterally into the CeA. Following recovery, animals were re-introduced to the respective experimental environment and underwent assessment of either reward learning (IntelliCage) or social abilities (Eco-HAB).

To measure the reduction of the MMP-9 activity in the CeA's of the TIMP-1-treated animals at the time equivalent to that of behavioral testing we used *in-situ* zymography illustrated with the confocal microscopy (x63) images. We show the depletion of the MMP-9 activity on the level of extracellular matrix surrounding the membranes of the cells within the

CeA, that further translates to the same effect observed on the level of the entire brain structure (Fig. S1). However, although, in-situ zymography is considered the most reliable method allowing for measuring MMP-9 activity with high specificity, its resolution is not equally satisfactory. Thus, we decided to perform identical series of experiments with a tool allowing for higher precision in localizing MMP-9 activity sites within the matrix surrounding cellular membranes, that is a small peptide biomarker (A580, Mw: 1769, Anaspec). This approach also clearly supports the notion that delivery of the TIMP-1 NPs into the CeA of both, *Fmr1* KO and WT animals, significantly depletes the activity of MMP-9 after 5 days from the injection into the animals' brains, as compared to the vehicle (BSA-loaded), control NPs (Fig. S2).

Reward learning

To investigate the effects of TIMP-1 treatment on cognition of *Fmr1* KO and control WT mice, we subjected them to a fully automated behavioral assessment in the IntelliCage system [47, 62]. IntelliCage is a spacious experimental cage housing up to 16 individually tagged mice. It is equipped with four conditioning units located in the corners of the cage. Each animal is identified by the readout of a radio frequency identification (RFID) electronic chip, which allows to program individual-specific experimental settings. IntelliCage system simultaneously records multiple parameters of mouse behavior, i.a. nosepokes, representing seeking behavior [47, 63]. In our protocol, mice first learned that water was accessible by nosepoking in each of the two holes located on the two different walls of each conditioning unit (Fig. 1b). Then access was limited to one conditioning unit per animal (max. 3 mice per corner, [50, 47, 62, 63]) to minimize the effects of social learning. In the subsequent 5-days-long reward learning phase, mice had access to water in one of the holes and to reward (10% sucrose solution) in the other [47, 64]. IntelliCage simultaneously records multiple parameters of mouse behavior. In this context it allowed for distinguishing between reward learning and reward palatability. The first reflected the rate at which animals gain the ability to efficiently obtain the reward, here measured as the number of instrumental responses (i.e. nosepoking into the appropriate hole upon entering the reward-containing conditioning unit, displayed as % of correct choices). The latter, evaluated the consumption of the reward, measured with the number of licks (indicating the amount of 10% sucrose solution drunk by each animal). Notably, once animals were successful in finding the reward there was no limit on its consumption, which enabled us to clearly differentiate between learning-dependent instrumental responses and reward-preference-dependent consumption. Additionally, the system reports locomotor activity and thus allows to control for its potential influence on learning. Performance was defined as a percentage of correct choices (nosepokes to the bottle containing sucrose) made immediately after entering the corner and measured over 5 days of training [47].

As optimal MMP-9 activity in the CeA is indispensable for the proper reward processing [47], reward learning is grossly impaired in *Fmr1* KOs (Fig. 1c, Fig. S3a, b). Moreover, during first 12h after reward introduction they present increased undirected nosepoking (reward seeking) [47, 64], further reflecting their poor learning capacity (Fig. S3b). These cognitive deficits are fully rescued by the targeted TIMP-1 treatment in the CeA (Fig. 1c, Fig. S4e).

In contrast, similar to previously shown data [47], injection of TIMP-1 in the CeA of the WT mice impairs their cognitive abilities (Fig. 1d), further confirming that optimal level of metalloproteinases activity is indispensable for reward learning. To exclude the possibility that the differences in reward learning were caused by different locomotion or reward palatability we compared activity (no. of visits to all corners) and reward consumption (no. of tube lickings and increase in licks when 10% sucrose was presented) in BSA- and TIMP-1-treated mice of both genotypes and found no differences (Fig. S4a, b, c, d; Fig. S6).

Social behavior

Mice were tested in Eco-HAB for 72h, protocol consisted of adaptation (48 h) and social behavior testing (24 h). During all phases of the experiment groups of 7 to 12 mice could freely explore all Eco-HAB compartments. During the test of social behavior, olfactory stimuli - bedding soaked with a scent of an unfamiliar mouse of the same strain, sex and age (novel social scent) or fresh bedding (novel non-social scent) were presented. Olfactory stimuli were placed behind the perforated partitions of the opposite testing compartments. Social approach was measured as a ratio of approach to social vs. non-social scents. In-cohort sociability, reflecting the tendency of mice for spending time together, was assessed during the 24h testing period.

Notably, injection of TIMP-1 releasing NPs to the CeA affected neither approach to social odor nor time voluntarily spent with cagemates, aspects of sociability we have previously showed [51] to be severely impaired in *Fmr1* KOs (Fig. 1f, g). Similarly, there was no impact of the treatment on social behavior of the WT mice (Fig. 1f, g), thus corroborating symptom-specificity of our approach.

Targeted TIMP-1 treatment normalizes impaired synaptic plasticity and morphology in the central amygdala of *Fmr1* KO mice

To test functional neuronal plasticity of the circuit, we measured long-term potentiation (LTP) at the basal amygdala-CeA pathway and observed that both the magnitude and stability of LTP are impaired in *Fmr1* KO mice (Fig. 2a, Fig. S3c). Injection of NPs releasing TIMP-1 to the CeA rescues those LTP deficits in *Fmr1* KOs (Fig. 2a), while having a detrimental effect on the LTP stability in the WT mice (Fig. 2b), mirroring the effects observed in reward learning experiments. These adverse effects of TIMP-1 in WTs corroborate our earlier findings [65]. Notably, treatment does not influence the properties of basic synaptic transmission in either of the genotypes (Fig. 2c, d, Fig. S7), highlighting that proposed strategy selectively targets plasticity, rather than basic synaptic function.

Further, the ultrastructure of the CeA is significantly altered in *Fmr1* KO mice (Fig. 3). The *Fmr1* KOs show significantly elevated number of synapses (Fig. 3 a). Moreover, CeA neurons in the *Fmr1* KOs have the elevated number of immature spines (Fig. S5b), synaptic shafts (Fig. S5c), and multi-innervated spines (Fig. S5 b-d, Fig. 3 d-i). However, in contrast to the findings from other brain structures [66, 67], the overall number of dendritic spines, and the number of mature spines in particular, is not different in the CeA of *Fmr1* KO and WT mice (Fig. 3 b, c; Fig. S5a).

We show that the targeted TIMP-1 treatment in *Fmr1* KOs normalizes a majority of the ultrastructural alterations in the CeA (Fig. 3). Specifically, TIMP-1 treatment lowers the number of immature spines and synaptic shafts to the control level (Fig. 3d, e). Coherently, it also restores the proportion of multi- to singly-innervated spines ([68], Fig. S5d) to that observed in the WT animals (Fig. 3f-h). The only parameter natively differing the *Fmr1* KOs from the WTs that is unchanged by the treatment is the overall number of synapses (Fig. 3a). On the other hand, the ultrastructure characteristics that do not differ between the genotypes, that is the overall number of dendritic spines and the number of mature spines, are increased by the TIMP-1 treatment in *Fmr1* KOs (Fig 3b, c).

Notably, TIMP-1 treatment in the WT animals results in similarly elevated levels of all dendritic spines and mature spines (Fig 3b, c). Moreover, as is observed in the *Fmr1* KOs, the treatment also causes a significant reduction in the number of immature spines and synaptic shafts (Fig. 3d, e) and does not change the overall number of synapses (Fig 3a). However, the application of TIMP-1 treatment in the WT mice has no effect on the proportion of multi- to singly-innervated spines (Fig. 3h, i).

In summary, with an exception of the overall number of synapses, targeted TIMP-1 treatment in the CeA of *Fmr1* KO mice normalizes all the ultrastructure parameters (no. of immature spines, shafts, and proportion of multi- to singly-innervated spines) that previously deviated from the WT levels.

Discussion

We show that the CeA-targeted TIMP-1 treatment, regulating synaptically overtranslated MMP-9 in *Fmr1* KO mice [7, 54], selectively rescues their cognitive impairments, while having no impact on the social deficits. The behavioral rescue is accompanied, and possibly caused, by the normalization of neuronal plasticity and synaptic ultrastructure of the CeA. Thus, we present a symptom- and circuit-specific approach, aimed at a particular molecular mechanism. Our results provide an insight into the molecular and neural mechanism of FXS pathophysiology, showing a causal link between TIMP-1-dependent neuronal plasticity in the CeA and cognitive deficits observed in that syndrome. The results also point to the therapeutic potential of the treatment, which can be tailored to the individual needs of FXS patients who exhibit different symptoms.Since TIMP-1 treatment resulting in subtle depletion of MMP-9 activity in *Fmr1* KOs caused a clear cognitive boost, while having an opposite effect in the WT animals, better understanding of TIMP-1 dose-dependency is needed to expedite translational efforts. Notably, the previously reported differences in MMP-9 levels under varying experimental conditions measured with gel zymography [33, 34, 55] were often more pronounced than our findings based on *in-situ* zymography, highlighting the dissimilarity of these two methods. The use of the *in-situ* zymography enabled us to accurately measure MMP-9 activity within the CeA, whose precise extraction for the purposes of gel zymography poses methodological challenges. However, the downside of this approach is the unfeasibility of relating the MMP-9 level to the activity of MMP-2. Thus, to solidify the conclusions drawn on the basis of zymography data, we employed a small peptide MMP-9 biomarker allowing for higher precision in localizing the enzyme's activity within the matrix surrounding cellular membranes. The results obtained

with both methods confirm the effectiveness of TIMP-1 in regulating MMP-9 activity *in situ* in the timeframe used for the assessment of behavioral phenotype rescue. However, more studies are needed to determine the optimal dosage, concentration, pharmacodynamics and protein release profiles of the TIMP-1-loaded designer nanoparticles *in situ*.

Even though some argue that TIMP-1 plays a dominant role in the inhibition of MMP-9, as does TIMP-2 in case of MMP-2 [69–72], the overall consensus in the field is that it is a non-selective metalloproteinases inhibitor and thus cannot be used to target activity of MMP-9 exclusively. Overall, the proteins from the TIMP family (TIMP-1 to -4) selectively inhibit different MMPs and members of the families Disintegrin and Metalloproteinase (ADAM) and Disintegrin and Metalloproteinase with Thrombospondin motifs (ADAMTS) [38, 73, 74]. Among them TIMP-1 is the most restrictive in its inhibitory range and has been shown to regulate most notably activity of the two gelatinases, MMP-2 and MMP-9, binding particularly strongly to the latter and its inactive form, pro-MMP-9 [75].

At the same time, numerous studies have shown that the overexpression of MMP-9, rather than MMP-2, plays a critical role in the manifestation of the symptoms characteristic to the *Fmr1* phenotype. Indeed, normalizing its levels leads to the amelioration of the behavioral and molecular deficits therein [14–16, 18–28]. Further, the cognitive disfunction related to reward learning we targeted with our therapeutic approach have been previously shown to depend specifically on the proper level of MMP-9 in the central amygdala [47]. For those reasons we argue, that even though one needs to consider that the applied TIMP-1 treatment may to some extent influence also the activity of MMP-2, such effects would not be critical for the amelioration of the symptoms in the *Fmr1* KO animals, especially in the context previously shown to be heavily dependent on the optimal levels of MMP-9. Additionally, to our knowledge there exists no other molecular tool that would allow for a more precise local targeting of MMP-9 activity than TIMP-1 designer NPs.

Moreover, the methods we used to measure MMP-9 activity are similarly burdened with non-specificity issue as both A580 MMP Substrate 1 and in-situ zymography may detect the activity of both MMP-2 and MMP-9. However, for the reasons mentioned in the previous paragraphs we consider them sufficient to draw conclusions focusing on the MMP-9 in the context of the *Fmr1* KO phenotype, as based on the numerous animal and human studies.

Taken together, even though the specificity of TIMP-1 inhibitory activity as well as specificity of A580 MMP Substrate 1 and in-situ zymography remain a problem, we argue that focus of this work on MMP-9 in the context of the *Fmr1* KO phenotype and reward learning is justified.

The evidence of TIMP-1-dependent facilitation of dendritic spine maturation and rescue of impaired LTP in *Fmr1* KOs, points to the fact that there exists a range of MMP-9 activity optimal for the proper synaptic plasticity, a notion coherent with previous studies [76]. However, there remain some notable gaps in our understanding of those processes. Notably, Wang et al. [76] showed that in hippocampus increased MMP-9 activity alone is sufficient to potentiate synapses and enlarge dendritic spines. At the same time, our data from WT animals with TIMP-1-depleted MMP-9 activity in the CeA shows the expected

opposite effect only in respect to the synapse potentiation, without a decrease in the size of the dendritic spines. Thus, more studies are needed to investigate a relationship between MMP-9 levels and dendritic spine maturation. Further, previous studies have shown that changing MMP-9 activity may alter long term plasticity without having any impact on other physiology measures, such as basic synaptic transmission or short time plasticity. For example, it has been shown that a non-selective MMP-9 inhibitor (GM6001) caused disruption of L-LTP without inducing changes in either short-term plasticity (measured as a paired-pulse ratio, PPF), or basic synaptic transmission [77]. The same authors showed that the L-LTP in brain slices obtained from the MMP-9 KO mice was destabilized, while basic synaptic transmission and PPF remained unchanged [77]. Our results showing that the TIMP-1 delivery to the CeA rescues the LTP in *Fmr1* KO animals without affecting basic synaptic transmission are in line with those discoveries.

In line with a rescue of impaired LTP in *Fmr1* KOs, it was also reported that an MMP-9 inhibitor (GM6001) increased maturation of dendritic spines and improved LTP in brain slices obtained from rats overexpressing MMP-9, animals with significant deficits in the LTP [78]. Interestingly, we have also found that a very slight increase in MMP-9 activity in the CeA of WTs reinforces motivation for sugar water ([79], *in review*). A similar motivational boost was also reported in the alcohol-consuming MMP-9 knock-out animals with CeA-restricted exogenous expression of the enzyme [80], which further solidifies the notion that a fine balance of the enzyme activity is needed for the correct reward processing.

Although the TIMP-1 treatment had significant impact on learning, circuit physiology and spine morphology in all tested animals, it did not influence the number of synapses that was significantly higher in *Fmr1 KO* mice. Moreover, in both *Fmr1* KO and WT animals TIMP-1 delivery into the CeA resulted in an increase in the number of the dendritic spines, which is usually regarded as an important neural correlate of learning and memory. As the effects of TIMP-1 treatment on behavioral performance and LTP in WT and *Fmr1* KOs animals differed, the data point out a more complex relationship between spine formation in the CeA and reward discrimination. We argue, that neural processes underlying reward learning are less dependent on the number of all the dendritic spines than on the right balance between the specific types of spines and other ultrastructure characteristics. This may include the number of the immature spines that are available for maturation and thus memory formation, and the number of synaptic shafts, which is critical for the function of the brain structures such as CeA, predominantly composed of inhibitory neurons. It is noteworthy, that both those measures were normalized to the WT control level after TIMP-1 treatment in *Fmr1* KOs, and markedly disrupted in the TIMP-1-treated WT animals, which points to their crucial role in the reward learning and LTP formation. This line of reasoning is in agreement with the previously described hypothesis of the optimal amount of the MMP-9 activity in the CeA necessary for the proper reward learning. Importantly, based on the performed experiments we only know that at the time of the LTP induction the level of all dendritic spines was higher in the TIMP-1-treated animals than in the respective control groups. However, we did not test if and how the induction of LTP influences maturation of the spines in TIMP-1-treated mice of both genotypes, and thus we are unable to tell if the usually observed phenomenon was absent in the TIMP-1-treated WT mice, who displayed impaired LTP and learning.

It was previously shown that *Fmr1* KO mice have a significantly elevated number of multi-innervated spines, which leads to the increased glutamate currents and hyperexcitability of neurons [81]. The multi-innervated spines are considered a basis of memory formation, engaging mechanisms alternative, and to some degree independent, from the classic synapse strengthening related to LTP [82]. Notably, it is argued that this mechanism of memory formation may be mobilized especially when LTP is blocked [68, 82, 83]. Additionally, it was shown that injecting animals with a blocker preventing changes in multi-innervation, disrupted memory formation only in old animals, in whom the mechanism was a major factor enabling learning [82]. Our data suggest that a similar mechanism may be at play in *Fmr1* KO mice treated with TIMP-1. Specifically, delivery of the MMP-9 inhibitor rescues BLA-CeA LTP and at the same time reduces the number of multi-innervated spines to the control levels. On the other hand, the same treatment in the WT mice, which have markedly lower levels of MMP-9, disrupts the LTP without increasing the number of the multi-innervated spines; which may stem from the fact that the disruption of LTP leads to the elevated multi-innervation only under specific circumstances and on a yet not fully understood time course, as suggested by the previous findings of Aziz et al. [82].

The lack of impact of the TIMP-1 treatment in the amygdala on social behavior might be considered unexpected. Although studies show that CeA circuits are crucial for choosing a context-appropriate reaction based on the information obtained via social interaction [84], engagement of MMP-dependent circuits within the CeA in social interaction has not been studied earlier. It is plausible that other, MMP-independent, mechanisms in the CeA are involved in social behaviors.

Moreover, the discoveries of Kim et al. indicate the diverse involvement of the neural circuits in the medial (CeM) and lateral (CeL) parts of CeA in reward processing [48]. Since the presented research examined the effects of the TIMP-1 delivery into the CeA without differentiating its medial and lateral parts the follow-up studies are needed to better understand the role of MMP-9 activity in those specific substructures in reward-motivated learning.

As we studied behavioral phenotypes in a social context in which males often become aggressive, we focused our studies on females. Importantly, earlier works show that behavioral impairments in *Fmr1* KOs are either equally pervasive in both sexes [85], or even more intense in females in terms of the typically autistic repetitive behaviors [86]. Additionally, as previously shown [51], *Fmr1* KO females display severe deficits in both cognition and social behavior, making them a suitable model to investigate the symptom-specific approach. Focusing on females whose autistic phenotype has been only rarely investigated offers an additional value. Such studies are highly needed in the face of the growing evidence that ASD and related mental disabilities are severely underdiagnosed in females [87–92]. Similarly, the problem of female underrepresentation in the phenotyping of the animal models of autism is a serious limitation of this research area. Ours findings are a scarce example of research investigating experimental therapeutic approach to autistic phenotype conducted in female subjects.

As of yet, in spite of billions of dollars being spent on research on neurodevelopmental disorders, scientists and clinicians have been struggling to propose effective targeted therapies [1]. Notably, in multiple cases phenotype rescue in the animal models has not been translated into effective treatment in patients. In the case of the FX patients application of minocycline, a drug repeatedly shown to normalize both, MMP-9 levels and behavioral performance in mice [15, 23, 24], turned only partially effective in improving cognitive function and only mildly helped in alleviating anxiety-related symptoms [93, 25, 94, 27]. Thus, the results reported here may not be of immediate clinical use, especially in face of the fact that FMRP protein regulates translation of over four hundred different mRNA in humans, and thus its disfunction influences multiple molecular pathways. However, we argue that since levels of MMP-9 and its role in different brain structures are very diverse, the application of the targeted approach, allowing for regulating multiple neural circuits crucial for a specific function (e.g. in the context of learning not only amygdala but also hippocampus, prefrontal cortex, nucleus accumbens, etc.), without influencing the off-target circuitry, may indeed be the key to success in regulating behavior.

Our research illustrates an innovative framework for evaluating mechanism-based treatments allowing to curtail problems notorious in assessment of new therapies, namely, low data replicability, species-inadequate assessment of phenotype and lack of accounting for individual differences in symptoms. Specifically, to assess effectiveness of the TIMP-1-based targeted therapy we employ fully automated and ecologically-relevant assays of mouse behavior; such systems mimic most important features of murine ecological niche and thus allow for measuring behaviors relevant for surviving and thriving under naturalistic conditions. Assessed behaviors are voluntary and unconstrained by time limits. Importantly, automated tests also assert high reproducibility of behavioral data due to the automation, standardized conditions and lack of human involvement in the process of testing. Moreover, they are computer-controlled and designed for evaluating behavior of individually-tagged, group-housed subjects, which eliminates confounding results related to social isolation [50, 62]. Thus, we present research exemplifying how combining cutting-edge methods in behavioral research and pharmacology leads to the efficient discovery of the symptom-, circuit- and mechanism-specific therapy, which can be further reliably tested in pre-clinical trials.

Supplementary Material

Refer to Web version on PubMed Central for supplementary material.

Acknowledgements

Funding

This work was supported by a grant from Switzerland through the Swiss Contribution to the enlarged European Union (PSPB-210/2010), European Research Council Starting Grant (H 415148), grants from the National Science Center (2013/08/W/NZ4/00691 and 2015/18/E/NZ4/00600), ‘BRAINCITY - Centre of Excellence for Neural Plasticity and Brain Disorders’ project of Foundation for Polish Science (FNP), and a Foundation for Polish Science (FNP) Team grant (Team/2016-1/6 to KN and LK). M.C. was supported by “Mobilność Plus”, a fellowship from Polish Ministry of Science and Higher Education grant number 1291/MOB/IV/2015/0. J.J.C. was supported by the National Science Center grant 2017/27/N/NZ1/01381.

References

1. Berry-Kravis EM, Lindemann L, Jønch AE, Apostol G, Bear MF, Carpenter RL, et al. Drug development for neurodevelopmental disorders: lessons learned from fragile X syndrome. Nat Rev Drug Discov. 2018; 17: 280–299. [PubMed: 29217836]
2. Bagni C, Tassone F, Neri G, Hagerman R. Fragile X syndrome: causes, diagnosis, mechanisms, and therapeutics. J Clin Invest. 2012; 122: 4314–4322. [PubMed: 23202739]
3. Hessl D, Tassone F, Loesch DZ, Berry-Kravis E, Leehey MA, Gane LW, et al. Abnormal elevation of FMR1 mRNA is associated with psychological symptoms in individuals with the fragile X premutation. Am J Med Genet Part B Neuropsychiatr Genet Off Publ Int Soc Psychiatr Genet. 2005; 139B: 115–121.
4. Hessl D, Grigsby J. Fragile X-associated tremor/ataxia syndrome: another phenotype of the fragile X gene. Clin Neuropsychol. 2016; 30: 810–814. [PubMed: 27355274]
5. Schneider A, Johnston C, Tassone F, Sansone S, Hagerman RJ, Ferrer E, et al. Broad autism spectrum and obsessive-compulsive symptoms in adults with the fragile X premutation. Clin Neuropsychol. 2016; 30: 929–943. [PubMed: 27355445]
6. NIMH » Research Domain Criteria (RDoC). Accessed 13 October 2020 https://www.nimh.nih.gov/research/research-funded-by-nimh/rdoc/index.shtml
7. Janusz A, Milek J, Perycz M, Pacini L, Bagni C, Kaczmarek L, et al. The Fragile X mental retardation protein regulates matrix metalloproteinase 9 mRNA at synapses. J Neurosci Off J Soc Neurosci. 2013; 33: 18234–18241.
8. Dziembowska M, Milek J, Janusz A, Rejmak E, Romanowska E, Gorkiewicz T, et al. Activity-dependent local translation of matrix metalloproteinase-9. J Neurosci Off J Soc Neurosci. 2012; 32: 14538–14547.
9. Dziembowska M, Wlodarczyk J. MMP9: a novel function in synaptic plasticity. Int J Biochem Cell Biol. 2012; 44: 709–713. [PubMed: 22326910]
10. Wójtowicz T, Mozrzymas JW. Matrix metalloprotease activity shapes the magnitude of EPSPs and spike plasticity within the hippocampal CA3 network. Hippocampus. 2014; 24: 135–153. [PubMed: 24115249]
11. Jasińska M, Miłek J, Cymerman IA, Łęski S, Kaczmarek L, Dziembowska M. miR-132 Regulates Dendritic Spine Structure by Direct Targeting of Matrix Metalloproteinase 9 mRNA. Mol Neurobiol. 2015. 1–12.
12. Vafadari B, Salamian A, Kaczmarek L. MMP-9 in translation: from molecule to brain physiology, pathology, and therapy. J Neurochem. 2016; 139 (Suppl 2) 91–114.
13. Beroun A, Mitra S, Michaluk P, Pijet B, Stefaniuk M, Kaczmarek L. MMPs in learning and memory and neuropsychiatric disorders. Cell Mol Life Sci CMLS. 2019; 76: 3207–3228. [PubMed: 31172215]
14. Bilousova TV, Rusakov DA, Ethell DW, Ethell IM. Matrix metalloproteinase-7 disrupts dendritic spines in hippocampal neurons through NMDA receptor activation. J Neurochem. 2006; 97: 44–56.
15. Bilousova TV, Dansie L, Ngo M, Aye J, Charles JR, Ethell DW, et al. Minocycline promotes dendritic spine maturation and improves behavioural performance in the fragile X mouse model. J Med Genet. 2009; 46: 94–102. [PubMed: 18835858]
16. Castagnola S, Bardoni B, Maurin T. The Search for an Effective Therapy to Treat Fragile X Syndrome: Dream or Reality? Front Synaptic Neurosci. 2017; 9: 15. [PubMed: 29163124]
17. Wen TH, Binder DK, Ethell IM, Razak KA. The Perineuronal 'Safety' Net? Perineuronal Net Abnormalities in Neurological Disorders. Front Mol Neurosci. 2018; 11: 270. [PubMed: 30123106]
18. Kokash J, Alderson EM, Reinhard SM, Crawford CA, Binder DK, Ethell IM, et al. Genetic reduction of MMP-9 in the Fmr1 KO mouse partially rescues prepulse inhibition of acoustic startle response. Brain Res. 2019; 1719: 24–29. [PubMed: 31128097]
19. Toledo MA, Wen TH, Binder DK, Ethell IM, Razak KA. Reversal of ultrasonic vocalization deficits in a mouse model of Fragile X Syndrome with minocycline treatment or genetic reduction of MMP-9. Behav Brain Res. 2019; 372 112068 [PubMed: 31271818]

20. Lovelace JW, Rais M, Palacios AR, Shuai XS, Bishay S, Popa O, et al. Deletion of Fmr1 from Forebrain Excitatory Neurons Triggers Abnormal Cellular, EEG, and Behavioral Phenotypes in the Auditory Cortex of a Mouse Model of Fragile X Syndrome. Cereb Cortex N Y N 1991. 2020; 30: 969–988.
21. Pirbhoy PS, Rais M, Lovelace JW, Woodard W, Razak KA, Binder DK, et al. Acute pharmacological inhibition of matrix metalloproteinase-9 activity during development restores perineuronal net formation and normalizes auditory processing in Fmr1 KO mice. J Neurochem. 2020; May 6. doi: 10.1111/jnc.15037
22. Sidhu H, Dansie LE, Hickmott PW, Ethell DW, Ethell IM. Genetic Removal of Matrix Metalloproteinase 9 Rescues the Symptoms of Fragile X Syndrome in a Mouse Model. J Neurosci. 2014; 34: 9867–9879. [PubMed: 25057190]
23. Rotschafer SE, Trujillo MS, Dansie LE, Ethell IM, Razak KA. Minocycline treatment reverses ultrasonic vocalization production deficit in a mouse model of Fragile X Syndrome. Brain Res. 2012; 1439: 7–14. [PubMed: 22265702]
24. Dansie LE, Phommahaxay K, Okusanya AG, Uwadia J, Huang M, Rotschafer SE, et al. Long-lasting effects of minocycline on behavior in young but not adult Fragile X mice. Neuroscience. 2013; 246: 186–198. [PubMed: 23660195]
25. Paribello C, Tao L, Folino A, Berry-Kravis E, Tranfaglia M, Ethell IM, et al. Open-label add-on treatment trial of minocycline in fragile X syndrome. BMC Neurol. 2010; 10: 91. [PubMed: 20937127]
26. Dziembowska M, Pretto DI, Janusz A, Kaczmarek L, Leigh MJ, Gabriel N, et al. High MMP-9 activity levels in fragile X syndrome are lowered by minocycline. Am J Med Genet A. 2013; 161A: 1897–1903. [PubMed: 23824974]
27. Leigh MJS, Nguyen DV, Mu Y, Winarni TI, Schneider A, Chechi T, et al. A randomized double-blind, placebo-controlled trial of minocycline in children and adolescents with fragile x syndrome. J Dev Behav Pediatr JDBP. 2013; 34: 147–155. [PubMed: 23572165]
28. Schneider A, Leigh MJ, Adams P, Nanakul R, Chechi T, Olichney J, et al. Electrocortical changes associated with minocycline treatment in fragile X syndrome. J Psychopharmacol Oxf Engl. 2013; 27: 956–963.
29. Gough A, Chapman S, Wagstaff K, Emery P, Elias E. Minocycline induced autoimmune hepatitis and systemic lupus erythematosus-like syndrome. BMJ. 1996; 312: 169–172. [PubMed: 8563540]
30. Lefebvre N, Forestier E, Farhi D, Mahsa MZ, Remy V, Lesens O, et al. Minocycline-induced hypersensitivity syndrome presenting with meningitis and brain edema: a case report. J Med Case Reports. 2007; 1: 22.
31. Ochsendorf F. Minocycline in Acne Vulgaris. Am J Clin Dermatol. 2010; 11: 327–341. [PubMed: 20642295]
32. Wright JW, Harding JW. Contributions of matrix metalloproteinases to neural plasticity, habituation, associative learning and drug addiction. Neural Plast. 2009; 2009 579382 [PubMed: 20169175]
33. Chaturvedi M, Figiel I, Sreedhar B, Kaczmarek L. Neuroprotection from tissue inhibitor of metalloproteinase-1 and its nanoparticles. Neurochem Int. 2012; 61: 1065–1071. [PubMed: 22892277]
34. Chaturvedi M, Molino Y, Sreedhar B, Khrestchatisky M, Kaczmarek L. Tissue inhibitor of matrix metalloproteinases-1 loaded poly(lactic-co-glycolic acid) nanoparticles for delivery across the blood-brain barrier. Int J Nanomedicine. 2014; 9: 575–588. [PubMed: 24531257]
35. Nothnick WB, Soloway P, Curry TE. Assessment of the Role of Tissue Inhibitor of Metalloproteinase-1 (TIMP-1) during the Periovulatory Period in Female Mice Lacking a Functional TIMP-1 Gene. Biol Reprod. 1997; 56: 1181–1188. [PubMed: 9160717]
36. Brew K, Dinakarpandian D, Nagase H. Tissue inhibitors of metalloproteinases: evolution, structure and function11Dedicated to Professor H. Neurath on the occasion of his 90th birthday. Biochim Biophys Acta BBA - Protein Struct Mol Enzymol. 2000; 1477: 267–283.
37. Okulski P, Jay TM, Jaworski J, Duniec K, Dzwonek J, Konopacki FA, et al. TIMP-1 abolishes MMP-9-dependent long-lasting long-term potentiation in the prefrontal cortex. Biol Psychiatry. 2007; 62: 359–362. [PubMed: 17210139]

38. Brew K, Nagase H. The tissue inhibitors of metalloproteinases (TIMPs): An ancient family with structural and functional diversity. Biochim Biophys Acta BBA - Mol Cell Res. 2010; 1803: 55–71.
39. Duan X, Chan C, Guo N, Han W, Weichselbaum RR, Lin W. Photodynamic Therapy Mediated by Nontoxic Core-Shell Nanoparticles Synergizes with Immune Checkpoint Blockade To Elicit Antitumor Immunity and Antimetastatic Effect on Breast Cancer. J Am Chem Soc. 2016; 138: 16686–16695. [PubMed: 27976881]
40. Aghebati-Maleki A, Dolati S, Ahmadi M, Baghbanzhadeh A, Asadi M, Fotouhi A, et al. Nanoparticles and cancer therapy: Perspectives for application of nanoparticles in the treatment of cancers. J Cell Physiol. 2020; 235: 1962–1972. [PubMed: 31441032]
41. He C, Duan X, Guo N, Chan C, Poon C, Weichselbaum RR, et al. Core-shell nanoscale coordination polymers combine chemotherapy and photodynamic therapy to potentiate checkpoint blockade cancer immunotherapy. Nat Commun. 2016; 7 12499 [PubMed: 27530650]
42. Castro F, Pinto ML, Pereira CL, Serre K, Barbosa MA, Vermaelen K, et al. Chitosan/γ-PGA nanoparticles-based immunotherapy as adjuvant to radiotherapy in breast cancer. Biomaterials. 2020; 257 120218 [PubMed: 32736253]
43. Serra P, Santamaria P. Nanoparticle-based autoimmune disease therapy. Clin Immunol. 2015; 160: 3–13. [PubMed: 25704658]
44. Kishimoto TK, Maldonado RA. Nanoparticles for the Induction of Antigen-Specific Immunological Tolerance. Front Immunol. 2018; 9
45. Serra P, Santamaria P. Nanoparticle-based approaches to immune tolerance for the treatment of autoimmune diseases. Eur J Immunol. 2018; 48: 751–756. [PubMed: 29427438]
46. Zampieri R, Brozzetti A, Pericolini E, Bartoloni E, Gabrielli E, Roselletti E, et al. Prevention and treatment of autoimmune diseases with plant virus nanoparticles. Sci Adv. 2020; 6 eaaz0295 [PubMed: 32494704]
47. Knapska E, Lioudyno V, Kiryk A, Mikosz M, Górkiewicz T, Michaluk P, et al. Reward learning requires activity of matrix metalloproteinase-9 in the central amygdala. J Neurosci Off J Soc Neurosci. 2013; 33: 14591–14600.
48. Kim J, Zhang X, Muralidhar S, LeBlanc SA, Tonegawa S. Basolateral to central amygdala neural circuits for appetitive behaviors. Neuron. 2017; 93: 1464–1479. e5 [PubMed: 28334609]
49. Murase S, Winkowski D, Liu J, Kanold PO, Quinlan EM. Homeostatic regulation of perisynaptic matrix metalloproteinase 9 (MMP9) activity in the amblyopic visual cortex. ELife. 2019; 8 e52503 [PubMed: 31868167]
50. Kiryk A, Mochol G, Filipkowski RK, Wawrzyniak M, Lioudyno V, Knapska E, et al. Cognitive abilities of Alzheimer's disease transgenic mice are modulated by social context and circadian rhythm. Curr Alzheimer Res. 2011; 8: 883–892. [PubMed: 22171952]
51. Puścian A, Łęski S, Kasprowicz G, Winiarski M, Borowska J, Nikolaev T, et al. Eco-HAB as a fully automated and ecologically relevant assessment of social impairments in mouse models of autism. ELife. 2016; 5 e19532 [PubMed: 27731798]
52. Fiala JC. Reconstruct: a free editor for serial section microscopy. J Microsc. 2005; 218: 52–61. [PubMed: 15817063]
53. Deerinck TJ, Bushong EA, Thor A, Ellisman MH, National Center for Microscopy and Imaging Research - NCMIR - National Center for Microscopy and Imaging Research. Accessed 22 May 2018
54. Gkogkas CG, Khoutorsky A, Cao R, Jafarnejad SM, Prager-Khoutorsky M, Giannakas N, et al. Pharmacogenetic inhibition of eIF4E-dependent Mmp9 mRNA translation reverses fragile X syndrome-like phenotypes. Cell Rep. 2014; 9: 1742–1755. [PubMed: 25466251]
55. Lovelace JW, Wen TH, Reinhard S, Hsu MS, Sidhu H, Ethell IM, et al. Matrix metalloproteinase-9 deletion rescues auditory evoked potential habituation deficit in a mouse model of Fragile X Syndrome. Neurobiol Dis. 2016; 89: 126–135. [PubMed: 26850918]
56. Gantois I, Khoutorsky A, Popic J, Aguilar-Valles A, Freemantle E, Cao R, et al. Metformin ameliorates core deficits in a mouse model of fragile X syndrome. Nat Med. 2017; 23: 674–677. [PubMed: 28504725]

57. Wen TH, Afroz S, Reinhard SM, Palacios AR, Tapia K, Binder DK, et al. Genetic Reduction of Matrix Metalloproteinase-9 Promotes Formation of Perineuronal Nets Around Parvalbumin-Expressing Interneurons and Normalizes Auditory Cortex Responses in Developing Fmr1 Knock-Out Mice. Cereb Cortex N Y N 1991. 2018; 28: 3951–3964.
58. Winiarski M, Borowska J, Wołyniak RM, Jędrzejewska-Szmek J, Kondrakiewicz L, Mankiewicz L, et al. Social learning about rewards - how information from others helps to adapt to changing environment. BioRxiv. 2021. 2021.03.09.434563
59. Klohs J, Baeva N, Steinbrink J, Bourayou R, Boettcher C, Royl G, et al. In Vivo Near-Infrared Fluorescence Imaging of Matrix Metalloproteinase Activity after Cerebral Ischemia. J Cereb Blood Flow Metab. 2009; 29: 1284–1292. [PubMed: 19417756]
60. Jeong S-R, Park H-Y, Kim Y, Lee K-W. Methylglyoxal-derived advanced glycation end products induce matrix metalloproteinases through activation of ERK/JNK/NF-κB pathway in kidney proximal epithelial cells. Food Sci Biotechnol. 2019; 29: 675–682. [PubMed: 32419966]
61. Takahashi C, Sheng Z, Horan TP, Kitayama H, Maki M, Hitomi K, et al. Regulation of matrix metalloproteinase-9 and inhibition of tumor invasion by the membrane-anchored glycoprotein RECK. Proc Natl Acad Sci. 1998; 95: 13221–13226. [PubMed: 9789069]
62. Puścian A, Łęski S, Górkiewicz T, Meyza K, Lipp H-P, Knapska E. A novel automated behavioral test battery assessing cognitive rigidity in two genetic mouse models of autism. Front Behav Neurosci. 2014; 8: 140. [PubMed: 24808839]
63. Puścian A, Winiarski M, Łęski S, Charzewski Ł, Nikolaev T, Borowska J, et al. Chronic fluoxetine treatment impairs motivation and reward learning by affecting neuronal plasticity in the central amygdala. Br J Pharmacol. 2021; 178: 672–688. [PubMed: 33171527]
64. Puścian A, Winiarski M, Łęski S, Charzewski Ł, Nikolaev T, Borowska J, et al. Chronic fluoxetine treatment impairs motivation and reward learning by affecting neuronal plasticity in the central amygdala. Br J Pharmacol. 2020; November 10. doi: 10.1111/bph.15319
65. Gorkiewicz T, Balcerzyk M, Kaczmarek L, Knapska E. Matrix metalloproteinase 9 (MMP-9) is indispensable for long term potentiation in the central and basal but not in the lateral nucleus of the amygdala. Front Cell Neurosci. 2015; 9: 73. [PubMed: 25814930]
66. Irwin SA, Galvez R, Greenough WT. Dendritic spine structural anomalies in fragile-X mental retardation syndrome. Cereb Cortex N Y N 1991. 2000; 10: 1038–1044.
67. De Toma I, Manubens-Gil L, Ossowski S, Dierssen M. Where Environment Meets Cognition: A Focus on Two Developmental Intellectual Disability Disorders. Neural Plast. 2016; 2016 4235898 [PubMed: 27547454]
68. Radwanska K, Medvedev NI, Pereira GS, Engmann O, Thiede N, Moraes MFD, et al. Mechanism for long-term memory formation when synaptic strengthening is impaired. Proc Natl Acad Sci U S A. 2011; 108: 18471–18475. [PubMed: 22025701]
69. Barton AK, Shety T, Bondzio A, Einspanier R, Gehlen H. Metalloproteinases and Their Tissue Inhibitors in Comparison between Different Chronic Pneumopathies in the Horse. Mediators Inflamm. 2015; 2015 569512 [PubMed: 26770019]
70. Chen G, Ge D, Zhu B, Shi H, Ma Q. Upregulation of matrix metalloproteinase 9 (MMP9)/ tissue inhibitor of metalloproteinase 1 (TIMP1) and MMP2/TIMP2 ratios may be involved in lipopolysaccharide-induced acute lung injury. J Int Med Res. 2020; 48 0300060520919592
71. Hou C, Miao Y, Wang X, Chen C, Lin B, Hu Z. Expression of matrix metalloproteinases and tissue inhibitor of matrix metalloproteinases in the hair cycle. Exp Ther Med. 2016; 12: 231–237. [PubMed: 27429651]
72. Sharov AA, Schroeder M, Sharova TY, Mardaryev AN, Peters EMJ, Tobin DJ, et al. Matrix Metalloproteinase-9 Is Involved in the Regulation of Hair Canal Formation. J Invest Dermatol. 2011; 131: 257–260. [PubMed: 20882038]
73. Jackson HW, Defamie V, Waterhouse P, Khokha R. TIMPs: versatile extracellular regulators in cancer. Nat Rev Cancer. 2017; 17: 38–53. [PubMed: 27932800]
74. Arpino V, Brock M, Gill SE. The role of TIMPs in regulation of extracellular matrix proteolysis. Matrix Biol. 2015; 44-46: 247–254. [PubMed: 25805621]

75. Cabral-Pacheco GA, Garza-Veloz I, Castruita-De la Rosa C, Ramirez-Acuña JM, Perez-Romero BA, Guerrero-Rodriguez JF, et al. The Roles of Matrix Metalloproteinases and Their Inhibitors in Human Diseases. Int J Mol Sci. 2020; 21 9739
76. Wang X, Bozdagi O, Nikitczuk JS, Zhai ZW, Zhou Q, Huntley GW. Extracellular proteolysis by matrix metalloproteinase-9 drives dendritic spine enlargement and long-term potentiation coordinately. Proc Natl Acad Sci U S A. 2008; 105: 19520–19525. [PubMed: 19047646]
77. Nagy V, Bozdagi O, Matynia A, Balcerzyk M, Okulski P, Dzwonek J, et al. Matrix metalloproteinase-9 is required for hippocampal late-phase long-term potentiation and memory. J Neurosci Off J Soc Neurosci. 2006; 26: 1923–1934.
78. Magnowska M, Gorkiewicz T, Suska A, Wawrzyniak M, Rutkowska-Wlodarczyk I, Kaczmarek L, et al. Transient ECM protease activity promotes synaptic plasticity. Sci Rep. 2016; 6 27757 [PubMed: 27282248]
79. Lebitko T, Dzik J, Jędrzejewska-Szmek J, Chaturvedi M, Jaworski T, Nikolaev T, et al. c-Fos-MMP-9 pathway in central amygdala mediates approach motivation but not reward consumption. BioRxiv. 2020. 2020.04.17.044792
80. Stefaniuk M, Beroun A, Lebitko T, Markina O, Leski S, Meyza K, et al. Matrix Metalloproteinase-9 and Synaptic Plasticity in the Central Amygdala in Control of Alcohol-Seeking Behavior. Biol Psychiatry. 2017; 81: 907–917. [PubMed: 28190519]
81. Booker SA, Domanski APF, Dando OR, Jackson AD, Isaac JTR, Hardingham GE, et al. Altered dendritic spine function and integration in a mouse model of fragile X syndrome. Nat Commun. 2019; 10 4813 [PubMed: 31645626]
82. Aziz W, Kraev I, Mizuno K, Kirby A, Fang T, Rupawala H, et al. Multi-input Synapses, but Not LTP-Strengthened Synapses, Correlate with Hippocampal Memory Storage in Aged Mice. Curr Biol. 2019; 29: 3600–3610. e4 [PubMed: 31630953]
83. Giese KP, Aziz W, Kraev I, Stewart MG. Generation of multi-innervated dendritic spines as a novel mechanism of long-term memory formation. Neurobiol Learn Mem. 2015; 124: 48–51. [PubMed: 25933505]
84. Andraka K, Kondrakiewicz K, Rojek-Sito K, Ziegart-Sadowska K, Meyza K, Nikolaev T, et al. Distinct circuits in rat central amygdala for defensive behaviors evoked by socially signaled imminent versus remote danger. Curr Biol. 2021; April 12. doi: 10.1016/j.cub.2021.03.047
85. Ding Q, Sethna F, Wang H. Behavioral analysis of male and female Fmr1 knockout mice on C57BL/6 background. Behav Brain Res. 2014; 271: 72–78. [PubMed: 24886775]
86. Nolan SO, Reynolds CD, Smith GD, Holley AJ, Escobar B, Chandler MA, et al. Deletion of Fmr1 results in sex-specific changes in behavior. Brain Behav. 2017; 7 e00800 [PubMed: 29075560]
87. Shattuck PT, Durkin M, Maenner M, Newschaffer C, Mandell DS, Wiggins L, et al. Timing of Identification Among Children With an Autism Spectrum Disorder: Findings From a Population-Based Surveillance Study. J Am Acad Child Adolesc Psychiatry. 2009; 48: 474–483. [PubMed: 19318992]
88. Russell G, Steer C, Golding J. Social and demographic factors that influence the diagnosis of autistic spectrum disorders. Soc Psychiatry Psychiatr Epidemiol. 2011; 46: 1283–1293. [PubMed: 20938640]
89. Dworzynski K, Ronald A, Bolton P, Happé F. How Different Are Girls and Boys Above and Below the Diagnostic Threshold for Autism Spectrum Disorders? J Am Acad Child Adolesc Psychiatry. 2012; 51: 788–797. [PubMed: 22840550]
90. Duvekot J, van der Ende J, Verhulst FC, Slappendel G, van Daalen E, Maras A, et al. Factors influencing the probability of a diagnosis of autism spectrum disorder in girls versus boys. Autism. 2016; December 9. doi: 10.1177/1362361316672178
91. Loomes R, Hull L, Mandy WPL. What Is the Male-to-Female Ratio in Autism Spectrum Disorder? A Systematic Review and Meta-Analysis. J Am Acad Child Adolesc Psychiatry. 2017; 56: 466–474. [PubMed: 28545751]
92. Ratto AB, Kenworthy L, Yerys BE, Bascom J, Wieckowski AT, White SW, et al. What About the Girls? Sex-Based Differences in Autistic Traits and Adaptive Skills. J Autism Dev Disord. 2018; 48: 1698–1711. [PubMed: 29204929]

93. Utari A, Chonchaiya W, Rivera SM, Schneider A, Hagerman RJ, Faradz SMH, et al. Side Effects of Minocycline Treatment in Patients With Fragile X Syndrome and Exploration of Outcome Measures. Am J Intellect Dev Disabil. 2010; 115: 433–443. [PubMed: 20687826]

94. Siller SS, Broadie K. Matrix Metalloproteinases and Minocycline: Therapeutic Avenues for Fragile X Syndrome. Neural Plast. 2012; 2012 e124548

Europe PMC Funders Author Manuscripts

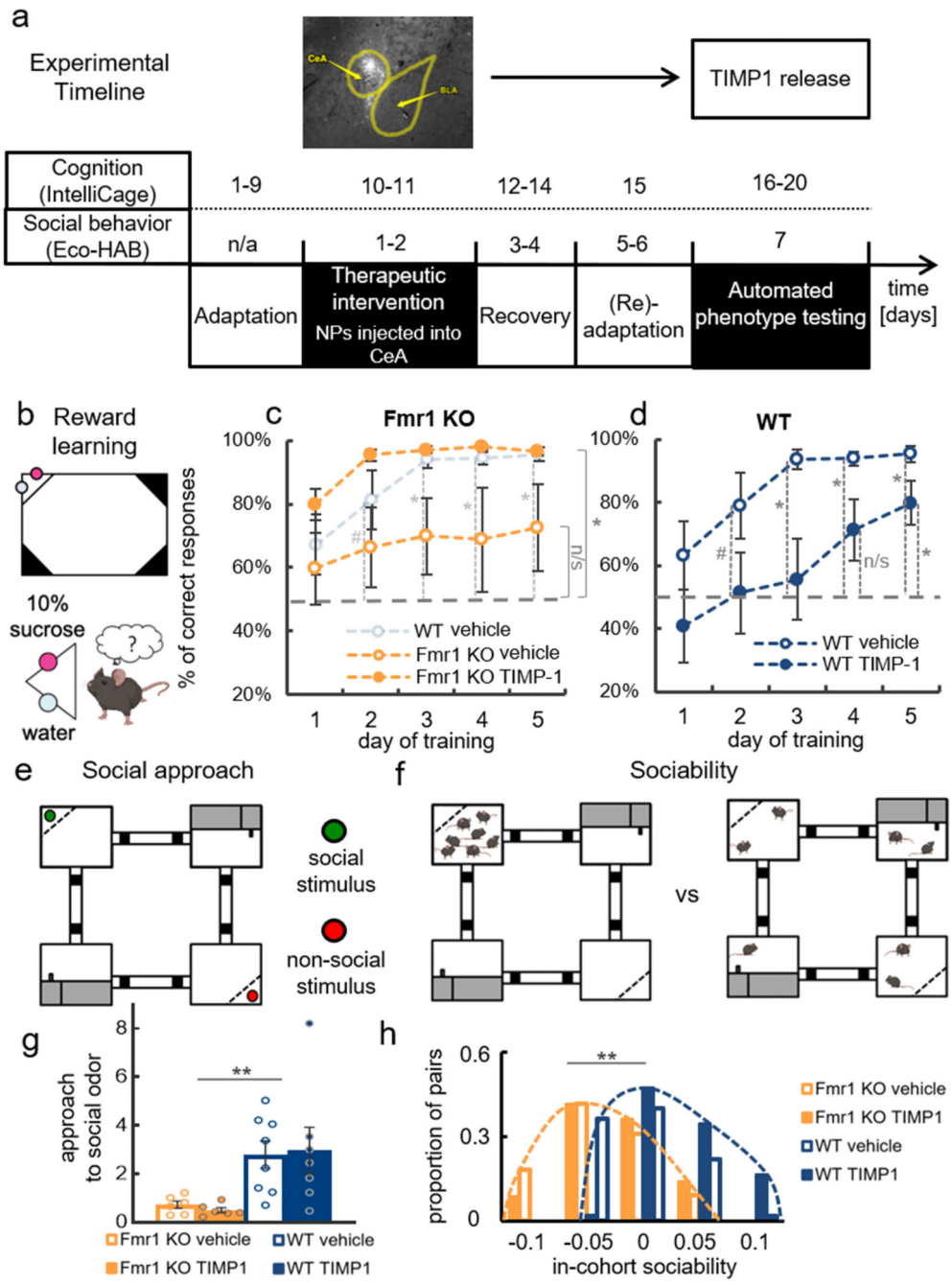

Fig. 1. TIMP-1 release in the CeA rescues cognitive but not social deficits in *Fmr1* KO mice.

(a) Mice were injected with the nanoparticles (NPs) releasing TIMP-1, an endogenous inhibitor of metalloproteinases; in the control condition animals were injected with the NPs releasing inactive protein, BSA (vehicle). Top left panel shows an example of the FITC-tagged NPs distribution in the CeA (x2). Experimental timeline highlights the peak of TIMP-1 release. **(b)** A schematic of the automated cognitive assessment in the IntelliCage system; during reward learning task the animals had to discriminate between bottles containing either sweetened (reward) or tap water (neutral stimulus). To assess reward

Europe PMC Funders Author Manuscripts

learning we measured the percentage of visits that began with a correct response (choice of the bottle with sweetened water). **(c)** Impaired learning of the *Fmr1* KO mice is fully rescued by the injection of NPs gradually releasing TIMP-1 to the CeA; corresponding performance of the WT controls (data as in D) shown in the background in light blue for comparison (TIMP-1 n=8; vehicle n=7). **(d)** TIMP-1 treatment impairs reward learning of control animals (TIMP-1 n=8; vehicle n=8). **(e)** Social abilities of the mice injected with the NPs releasing TIMP-1 to the CeA as tested in the Eco-HAB system. Approach to novel social stimulus (**f**) and in-cohort sociability (**g**) are unaffected in either of the groups, socially impaired *Fmr1* KOs or WT controls (*Fmr1* KO TIMP-1 n=6, vehicle n=6; WT TIMP-1 n=5; vehicle n=8). Dots and bars represent actual data, while dashed lines serve to guide the eye. Data are mean values and error bars represent SEM, $^{\#}$ $p<0.1$, * $p<0.05$, ** $p<0.01$ (c, d - Wilcoxon signed-rank test, performance compared to chance level represented by the horizontal dashed line; f - Mann-Whitney U-test; g – KS test). CeA – central amygdala, BL - basolateral amygdala.

Europe PMC Funders Author Manuscripts

Europe PMC Funders Author Manuscripts

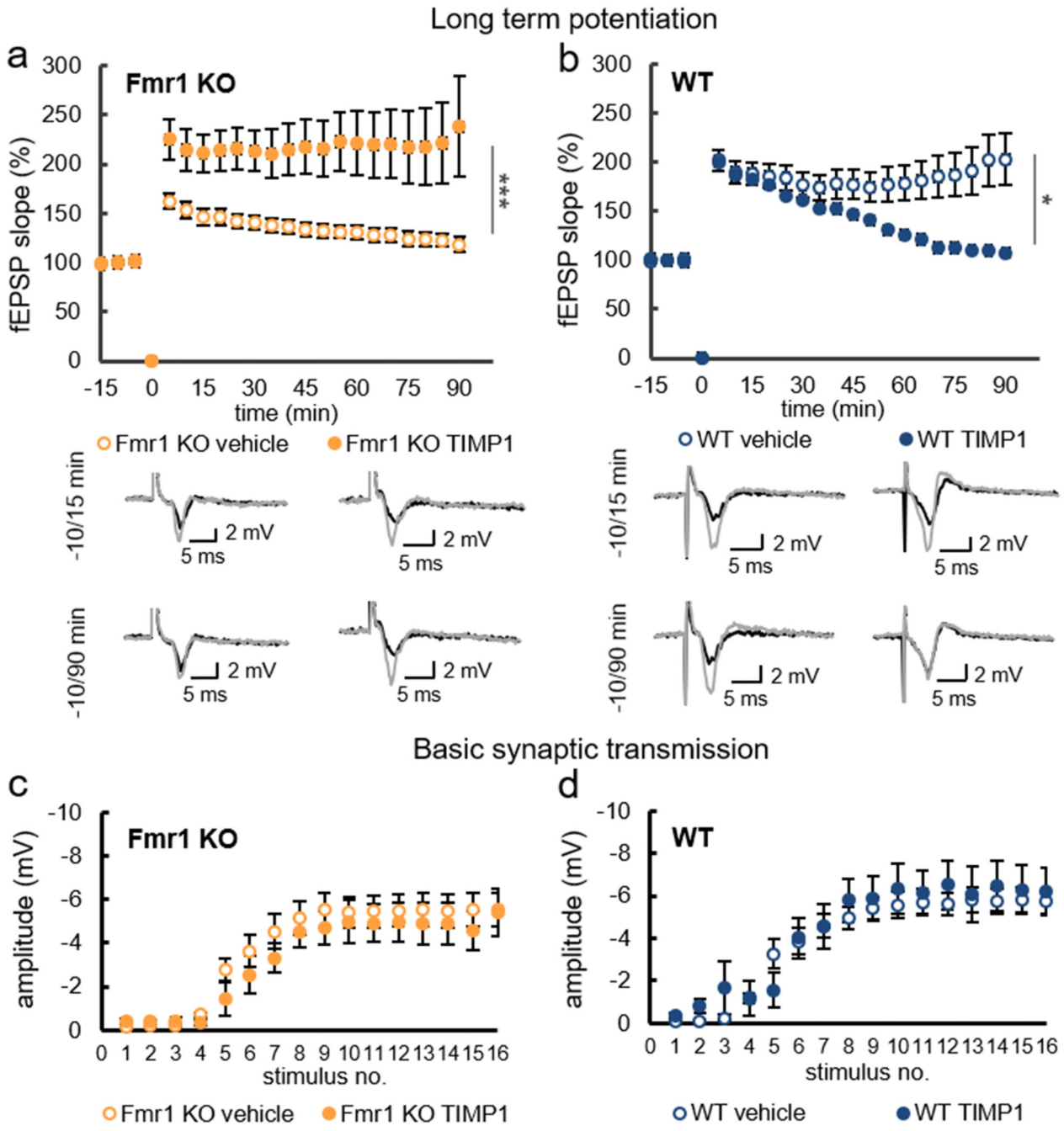

Fig. 2. TIMP-1 release in the CeA normalizes impaired functional synaptic plasticity of *Fmr1* KO mice.

Long term potentiation was induced at the basal amygdala – central amygdala (BA-CeA) pathway. **(a)** Impaired LTP of *Fmr1* KO mice is fully rescued by the injection of the TIMP-1 releasing NPs (TIMP-1 group, 7 animals, n=9 slices; CTRL group 7 animals, n=11 slices). (**b**) TIMP-1 treatment in WT mice results in LTP instability (TIMP-1 group, 6 animals, n=7 slices; CTRL group, 8 animals, n=9 slices). (**c, d**) There are no differences in the basic synaptic transmission properties (input-output curves) between genotypes or treatments

(*Fmr1* KO TIMP-1 group, 7 animals, n=7 slices; *Fmr1* KO CTRL group, 7 animals, n=11 slices; WT TIMP-1 group, 6 animals, n=7 slices; WT CTRL group, 8 animals, n=10 slices). Data are mean values and error bars represent SEM, *** $p<0.001$ (Two-way RM ANOVA, a - $F(1,18) = 20.41$, $p=0.0003$; b - $F(1, 14) = 4.896$, $p=0.0440$; c - $F(1, 16) = 0.9620$, $p=0.3413$; d - $F(1, 15) = 0.2618$, $p=0.6164$). Examples of fEPSP traces recorded 10 min before (black) and 15/90 min after (gray) induction of the LTP. Scale bars = 0.2 mV and 5ms.

Europe PMC Funders Author Manuscripts

Europe PMC Funders Author Manuscripts

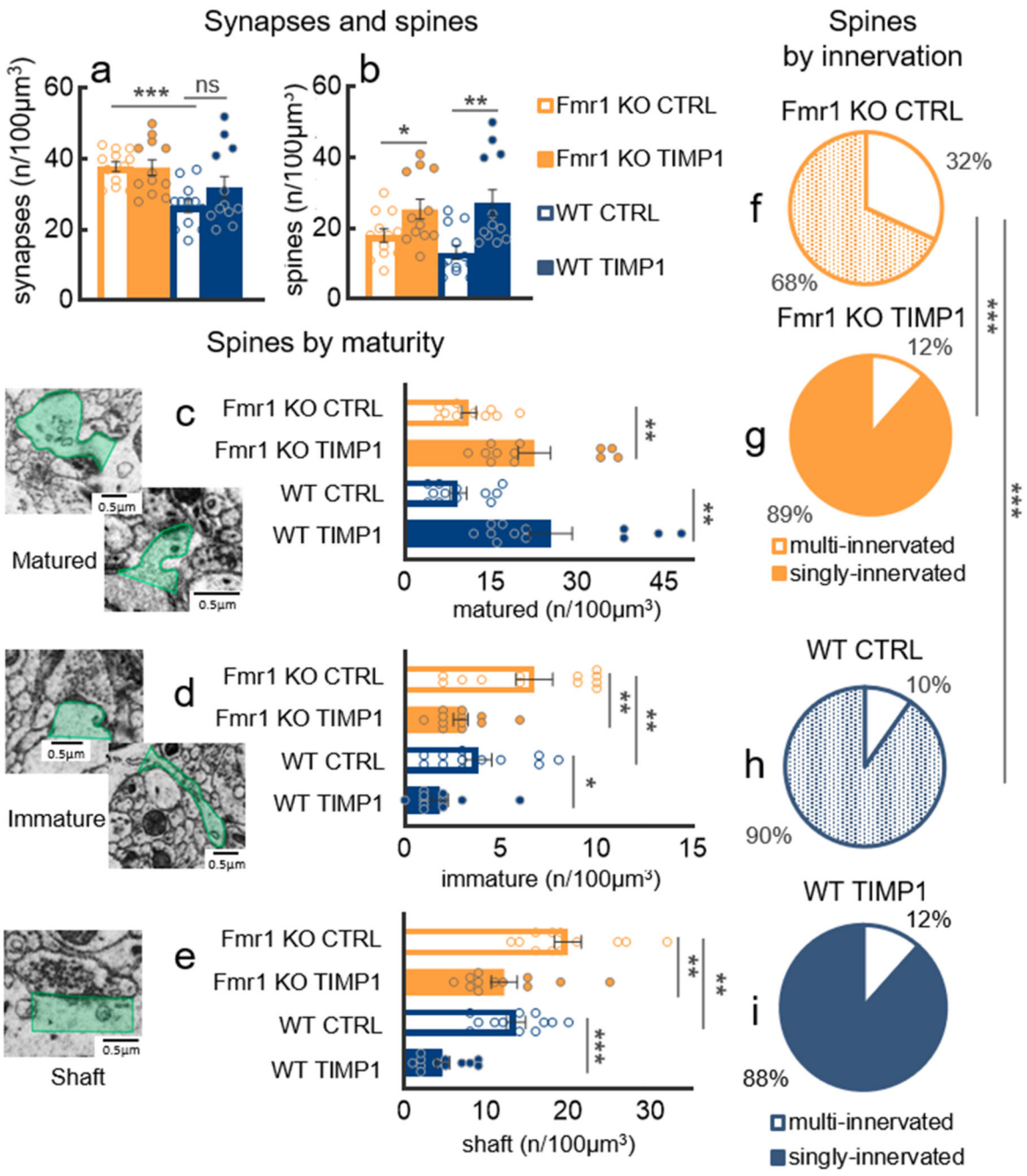

Fig. 3. TIMP-1 release in the CeA normalizes synaptic morphology of *Fmr1* KO mice.

(**a**) The overall number of synapses, elevated in *Fmr1* KO mice, is not changed by the TIMP-1 treatment in either controls or mutants. (**b**) The number of dendritic spines, which does not differ in *Fmr1* KO and WT mice, increases after TIMP-1 injection in both groups. (**c**) Similarly, the number of matured spines, identical in *Fmr1* KOs and WTs, increases due to the TIMP-1 treatment. In contrast, in TIMP-1-treated *Fmr1* KO mice the elevated number of (**d**) immature spines and (**e**) shaft synapses, decreases to the level observed in WTs. Gradual release of TIMP-1 also reduces the number of immature spines and shafts in WT

mice. (**f, g**) The TIMP-1 treatment restores the proportion of the multi- to singly-innervated spines in *Fmr1* KO mice to that observed in WT animals (**h**) and does not influence proportion of multi- to singly-innervated spines in WT mice (**i**). 12 cubic samples imaged per group (3 per each animal); F*mr1* KO TIMP-1, n=3, CTRL, n=3; WT TIMP-1, n=3, CTRL, n=3. Data are mean values and error bars represent SEM, * $p<0.05$, ** $p<0.01$, *** $p<0.001$ (a, b, c, d, e – t-test for independent samples, Mann-Whitney U-test; f, g, h, i - chi-squared test).

Europe PMC Funders Author Manuscripts